# Highly efficient terahertz radiation from a thin foil irradiated by a high-contrast laser pulse

Z. Jin,[1,*] H. B. Zhuo,[2,3,†] T. Nakazawa,[4] J. H. Shin,[4] S. Wakamatsu,[4] N. Yugami,[5] T. Hosokai,[1] D. B. Zou,[2] M. Y. Yu,[6] Z. M. Sheng,[3,7,8] and R. Kodama[1,4,9]

[1]*Photon Pioneers Center, Osaka University, 2-1 Yamada-oka, Suita, Osaka, 565-0871, Japan*

[2]*College of Science, National University of Defense Technology, Changsha 410073, People's Republic of China*

[3]*Collaborative Innovation Center of IFSA, Shanghai Jiao Tong University, Shanghai 200240, People's Republic of China*

[4]*Graduate School of Engineering, Osaka University, 2-1 Yamada-oka, Suita, Osaka, 565-0871, Japan*

[5]*Department of Advanced Interdisciplinary Sciences, Center for Optical Research & Education, and Optical Technology Innovation Center, Utsunomiya University, Yoto 7-1-2, Utsunomiya, Tochigi, 321-8585, Japan*

[6]*Institute for Fusion Theory and Simulation and Department of Physics, Zhejiang University, Hangzhou 310027, People's Republic of China and Institute of Theoretical Physics I, Ruhr University, D-44780 Bochum, Germany*

[7]*SUPA, Department of Physics, University of Strathclyde, Glasgow G0 4NG, United Kingdom*

[8]*Key Laboratory for Laser Plasmas (Ministry of Education) and Department of Physics and Astronomy, Shanghai Jiao Tong University, Shanghai 200240, People's Republic of China*

[9]*Institute of Laser Engineering, Osaka University, 2-6 Yamada-oka, Suita, Osaka, 565-0871, Japan*

(Received 3 February 2016; revised manuscript received 27 April 2016; published 21 September 2016)

Radially polarized intense terahertz (THz) radiation behind a thin foil irradiated by ultrahigh-contrast ultrashort relativistic laser pulse is recorded by a single-shot THz time-domain spectroscopy system. As the thickness of the target is reduced from 30 to 2 μm, the duration of the THz emission increases from 5 to over 20 ps and the radiation energy increases dramatically, reaching ∼10.5 mJ per pulse, corresponding to a laser-to-THz radiation energy conversion efficiency of 1.7%. The efficient THz emission can be attributed to reflection (deceleration and acceleration) of the laser-driven hot electrons by the target-rear sheath electric field. The experimental results are consistent with that of a simple model as well as particle-in-cell simulation.

DOI: 10.1103/PhysRevE.94.033206

Interaction of ultraintense laser pulse with solid foil target produces high fluxes of energetic electrons that can lead to secondary processes such as bright x-ray and $\gamma$-ray emission [1], ion acceleration [2,3], and powerful terahertz (THz) radiation [4–9]. The mechanisms involved are of basic research interest in high-energy density physics and the resulting particle bunches and radiation have many novel applications [1–9]. Powerful THz radiation has been detected at both the front and rear sides of the targets. Several mechanisms of THz emission from the target front have been proposed, including that of transient electron currents driven by the ponderomotive force [4], the antenna effect [6], and surface electron currents [8]. However, an explanation for the recently reported [10] extremely powerful THz pulses emitted from the rear-target surface is still lacking. It has been suggested that the radiation could be from the target-rear electron sheath, which is also responsible for target normal sheath acceleration (TNSA) of ions [3]. In this model, a hot relativistic MeV electron bunch created by the laser impact is reflected by the intense sheath fields on both sides of the target. Dipolelike acceleration- and deceleration-induced radiation (bremsstrahlung) is thus emitted.

In this paper we report experimental results on efficient, namely, up to 1.7% laser-to-THz energy conversion efficiency, generation of radially polarized THz radiation up to 10.5 mJ per pulse behind a thin solid target irradiated by intense ultrahigh-contrast laser. It is found that decrease of the target thickness from 30 to 2 $\mu$m results in more than threefold enhancement of the THz radiation energy. A simple theoretical model, confirmed by particle-in-cell (PIC) simulation, shows that for thin targets the hot electrons are refluxed between the front and rear sheaths. As a result, the sheath electron density and the sheath field intensity are enhanced, leading to longer emission duration and thus higher THz energy. The observed angular distribution and temporal profile of the THz radiation also agree with this argument.

Our experiments make use of the P-Cube laser system at the Graduate School of Engineering at Osaka University [7]. The laser pulse duration $\tau_L$ and wavelength $\lambda_0$ after compression, monitored during the experiment, are about 30 fs and 800 nm, respectively. A saturable absorber is used to achieve a laser intensity contrast ratio of $10^{-10}$. As illustrated in Fig. 1(a), the $p$-polarized laser is focused to a full width at half maximum spot of ∼6 $\mu$m at 45° incidence on a Cu target. The focused laser energy $E_L$ can be varied from 150 to 600 mJ by tuning the pump energy of the amplifiers. The peak laser intensity on target is $I_L \sim (0.88\text{–}3.5) \times 10^{19}$ W/cm$^2$. The THz radiation is sent to a calibrated Golay cell coupled with a polyethylene THz polarizer for measuring the THz energy and polarization. A single-shot THz time-domain spectroscopy (TDS) system with direct spatial encoding pump-probe electro-optical sampling [10] is developed for this experiment. It enables us to obtain the temporal wave profile with a resolution of ∼94.3 fs and a total time window of ∼37.7 ps. Polymer and THz long-pass filters are used to block any visible and near-infrared radiation at wavelengths less than 20 μm. The probe beam, which is reflected by two aluminum echelons to produce 400 (20 × 20) beamlets with different time delays, is collinearly focused onto a 1-mm-thick ⟨110⟩ ZnTe crystal along with the synchronized THz pulse. As shown in Fig. 1(b), the THz radiation is detected by the TDS system and plasma expansion from both sides of

*jin-z@ppc.osaka-u.ac.jp
†hongbin.zhuo@gmail.com

 

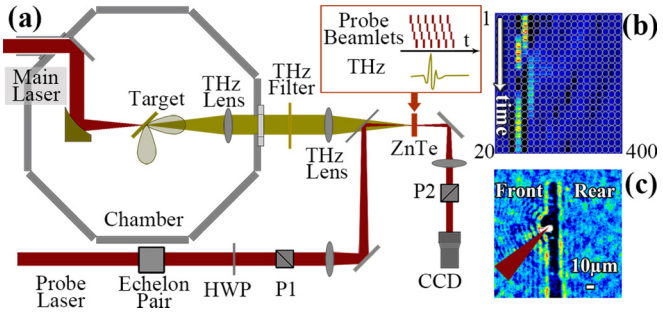


FIG. 1. (a) Experimental setup. The THz radiation emitted from the target rear is collected and sent to a calibrated THz energy meter or to a single-shot TDS system with a dual reflective echelon pair. The beamlets produced by the echelon pair arrive at the ZnTe at different time delays to the THz pulse. Via the electro-optic effect induced by the THz electric field, the temporal evolution of the THz field is encoded with respect to the intensity of each beamlet. (b) Typical modulated intensity of the 400 ($20 \times 20$) beamlets, obtained by comparing the difference between images on the CCD with and without the THz pulse. (c) Image of the plasma expansion at 40 ps after the arrival of the main laser beam at the target, monitored using a pump-probe shadowgraph system.

the target is also monitored by a pump-probe shadowgraph system. Figure 1(c) shows that there is no observable plasma expansion at the rear surface.

Runs for different laser energies and target thicknesses were carried out. An important result obtained is the strong dependence of the THz radiation energy on the target thickness. The energy and temporal profiles of the THz radiation with horizontal polarization emitted along an angle 45° from the target normal in the horizontal plane were measured by the Golay cell and the TDS system. Figure 2 gives the measured THz energy emitted 45° from the target normal for the laser energies 600, 450, 320, and 240 mJ and target thicknesses $D$ from 30 to 2 $\mu$m. As we can see, a decrease of the target thickness results in an increase of the THz radiation energy. One can also see that the variation depends on the laser energy: For $E_L \geqslant 450$ mJ, the THz energy first increases slowly as the target thickness is reduced from 30 to 5 $\mu$m and it then rises

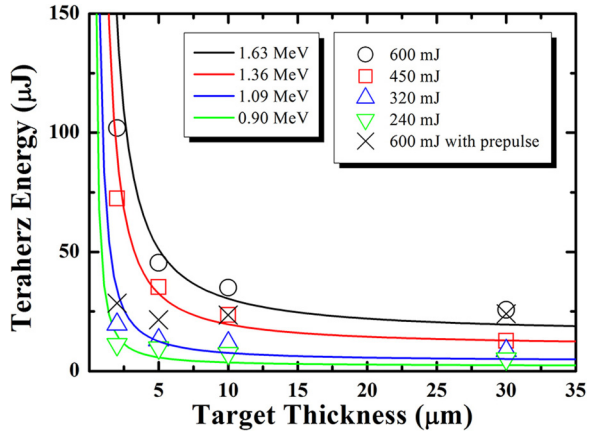


FIG. 2. Terahertz radiated energy versus target thickness for different electron temperatures. The solid curves are from the theoretical model.

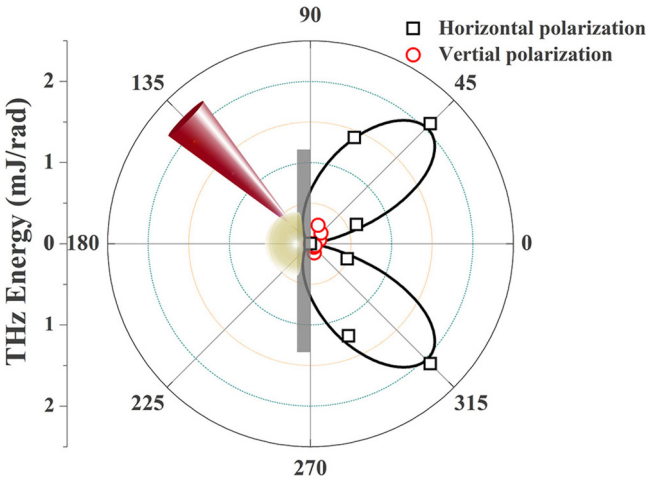


FIG. 3. Angular distribution of THz energy measured by changing the position of the THz lens inside the chamber. The black curves are for the best-fit dipole emission pattern.

quickly as the target thickness is reduced from 5 to 2 $\mu$m. However, for $E_L \leqslant 320$ mJ, there is only a little increase of the THz energy as the target thickness is reduced to 2 $\mu$m. These results are very similar to the dependence of the TNSA proton energy on the target thickness [3], indicating strong correlation between the THz emission and TNSA.

The angular distribution of the THz radiation emitted from the 2-μm target-rear surface for a 600-mJ laser pulse has a typical dipolelike radiation pattern, which is consistent with the theory [11] and supports the argument that sheath bremsstrahlung dominates the THz radiation process. As shown in Fig. 3, where the black squares are for the horizontally polarized THz energy $E_H$ and the red circles for the vertically polarized THz energy $E_V$, with the latter close to the noise level, the angular distribution of the THz energy has two symmetrical peaks at 45° and 315° to the target normal and the field is mainly horizontally polarized with $E_H/E_V > 10$ at 45°. In order to see the three-dimensional characteristics, the radiation in the vertical plane is also recorded. The polarizations are perpendicular (also with $E_V/E_H > 10$ at 45°) and almost identical to that in the horizontal plane. These polarization characteristics indicate that the THz radiation is mainly radially polarized, which is consistent with the optical observation in Ref. [12]. The peak THz energy at 45° is 102 $\mu$J, with a collection solid angle of 0.0485 sr. Assuming a radially symmetric cone dipole structure of radiation, one can estimate that the total energy emitted into the $2\pi$ solid angle is 10.5 mJ, corresponding to a laser-to-THz radiation conversion efficiency of 1.7%. This is about an order of magnitude higher than the existing results [11].

We now consider the temporal characteristics of the target-back THz radiation. Figures 4(a)–4(d) shows typical profiles of the THz radiation as recorded by the TDS system for various target thicknesses. The peak THz field on the ZnTe crystal is calibrated at ~40 MV/m [13], which confirms the Golay cell energy measurement discussed above. For $D > 2$ $\mu$m, THz radiation starts as a subpicosecond sharp single-cycle spike, followed by ~10-ps disordered low-frequency fluctuations. The corresponding spectrum is broad and multipeaked. In

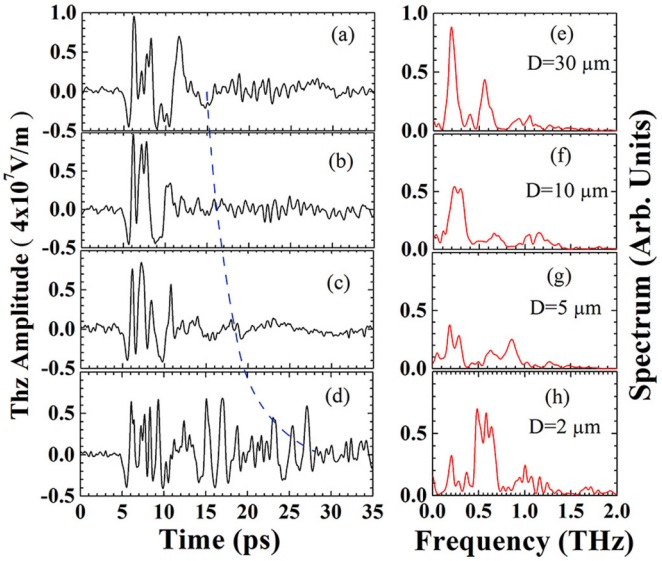


FIG. 4. (a)–(d) Experimentally detected THz time-domain electric field waveforms and (e)–(h) corresponding spectrum from Cu targets with different thickness. The laser energies used here are fixed at 600 mJ. The blue dashed line gives the calculated sheath lifetime $\sim(N_r + 1)$.

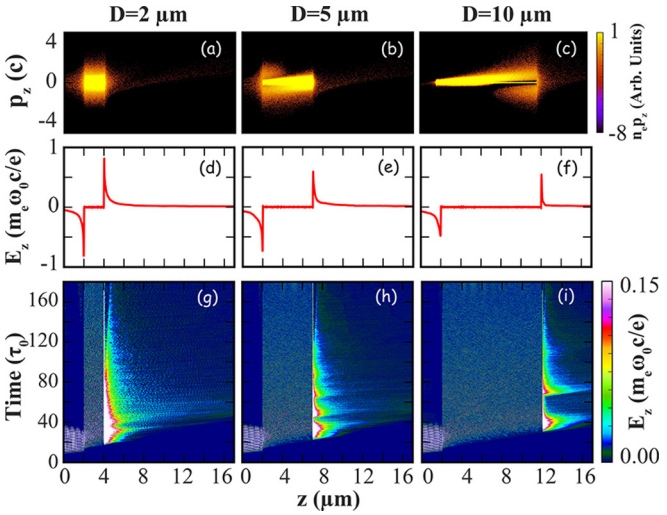


FIG. 5. Two-dimensional PIC simulation results. (a)–(c) Electron momentum phase space $p_z - z$ and (d)–(f) sheath electric field $E_z$ along the target center for three thickness targets at $t = 40$ laser periods. (g)–(i) Time evolution of the sheath electric field $E_z$ for three thickness targets.

contrast, for $D = 2\,\mu$m, the THz radiation lasts for $\sim$25 ps, with regular oscillating structure at about 0.5 THz. We note that the duration of the measured THz radiation is much longer than that of the laser pulse, which implies that it is closely associated with the long-time sheath evolution. The significant difference between these two cases can be attributed to the fact that the target-back sheath decays much faster for thicker targets.

The experimental results can be understood in terms of the TNSA mechanism for acceleration target-back ions [3,14]. The hot electrons generated at the front surface by the laser can propagate easily through the target, enter the rear vacuum, and form a thin sheath, whose electrostatic space-charge field rapidly becomes strong enough to reflect the still entering high-energy electrons. The reflected electrons reaching the front sheath are in turn reflected and the reflection process continues. Consequently, the density of the electron in the rear sheath surface is the sum of that from laser-accelerated new electrons and that reentering the target at intervals of the refluxing time [3]. It therefore depends strongly on the laser pulse duration and the target thickness. As the refluxing period is roughly $\tau_F \sim 2D/v_h$, where $D$ is the target thickness and $v_h$ an average velocity of the hot electrons in the normal direction, the average sheath electron density $n_e$ on the rear surface can be roughly estimated as $n_e \propto (N_r + 1)$, where $N_r \sim \tau_L/\tau_F$ is the average number of refluxing within the laser pulse duration $\tau_L$. For thin targets we have $\tau_F \ll \tau_L$, so $N_r$ can be rather large and $n_e$ can be significantly enhanced.

Two-dimensional simulations are performed using the PIC code described in Ref. [15] using the same laser pulse intensity, wavelength, duration, polarization, and incidence angle as in the experiments. The target is a quasineutral plasma slab containing $Cu^{4+}$ ions and electrons of density $n_e = 40n_c$ and temperature 1 keV. The target thickness varies from 2 to 10 $\mu$m. The simulation box is $60 \times 30\,\mu\text{m}^2$ with spatial resolution up to 100 cells per wavelength. Absorbing boundary conditions on all sides of the simulation box are adopted for both electromagnetic waves and particles. Due to the limited computing resource, the simulations only reproduce the early stage (within a few picoseconds) after laser target interaction, which is not sufficient to demonstrate the long-time sheath evolution and the THz radiation process. However, since the refluxing enhancement takes place within the laser time duration, the simulation results can straightly give us the evidence of the electron generation, refluxing, and the necessary information of the sheath field formed on the rear surface.

Figure 5 shows the longitudinal phase spaces of the electrons and the distribution of the axial electric field at $t = 40\tau_L$ for three target thicknesses, as well as the corresponding evolution of the axial electric field. One can see from the top and bottom rows of the panels that at $t = 40\tau_L$, the hot electrons have already refluxed several times in the 2-$\mu$m target, just completed their first refluxing in the 5-$\mu$m target, and are just being reflected by the rear sheath field in the 10-$\mu$m target. Figures 5(d)–5(f) show that the maximum sheath electric field at this time for the 2-$\mu$m target is 1.42 and 2.0 times that for the 5- and 10-$\mu$m targets, respectively. Figures 5(g)–5(i) for the temporal evolution of the axial sheath electric field show that the rear sheath field of the thinnest target is much more homogeneous and long lasting. Accordingly, a thin target can produce THz radiation with longer duration and higher energy. In contrast, for the two thicker targets, the sheath field contains large gaps and gradients associated with the distinct reflection events since the hot electrons take more time to traverse the target. The distortion in the temporal profile of the THz radiation and the complex spectral distribution for the thick target cases shown in Fig. 3 may be attributed to the irregular behavior of the sheath electric field.

The refluxing enhancement effect ends with the laser pulse, while the radiation is excited during the long-time sheath

evolution. For simplicity, we model the electrostatic sheath formed at the target-rear surface as an accelerating dipole [11], the radiated power can then be expressed as [16]

$$\frac{dP}{d\Omega} = \frac{e^2\dot{v}^2}{4\pi c^3}\frac{\sin^2\theta}{(1-v\cos\theta/c)^5}, \quad (1)$$

where $e$ is the electron charge, $\theta$ is the angle between the target normal and the detector, and $v$ and $\dot{v}$ are the electron velocity and acceleration and deceleration normal to the target surface, respectively. The acceleration is directly proportional to the electrostatic sheath field $E_s$, which scales as $E_s \propto (n_e T_e)^{1/2}$. The width of the sheath should be of the order of the Debye length $\lambda_D = (T_e/4\pi e^2 n_e)^{1/2}$, so the total radiated power, proportional to the square of the number of electrons in the sheath $N_e \propto n_e \lambda_D$, increases as $(N_r+1)^2$. That is, it becomes larger as the target thickness is reduced.

In their refluxing the hot electrons suffer energy loss from collisions with the target particles [17]. The sheath lifetime for different target thicknesses can be calculated from the stopping-power data from the NIST database [18], which roughly scale as $\tau_{\text{sheath}} \propto D^{-1} \propto (N_r+1)$. As shown in Fig. 4, the sheath lifetime shown as the blue dashed curve is consistent with our experimental results. It is found that in a thick target an electron can lose its energy rapidly. For the parameters of our experiments, the ponderomotive force is mainly responsible for the hot-electron generation and acceleration. Accordingly, the electron temperatures estimated from the ponderomotive energy scaling [19] are 1.63, 1.36, 1.09, and 0.90 MeV, respectively, for the laser energies 600, 450, 320, and 240 mJ. The corresponding THz radiation energy $P\tau_{\text{sheath}}$, roughly proportional to $(N_r+1)^3$ according to the above analysis, is shown in Fig. 2 by the solid curves. We see that the fit with the experimental results is quite good. Moreover, the radiation energy increases rapidly as the target thickness decreases to below $D \sim 0.5 v_h \tau_L \sim 5\ \mu$m, where the hot-electron refluxing time becomes shorter than the laser duration, so the refluxing electrons can be multiply accelerated by the laser.

High laser contrast is crucial for efficient generation of the THz radiation, as it prevents formation on the front surface of an expanding preplasma. The latter increases the effective target thickness and thereby hampers the formation of an intense sheath at the back of an originally thin target [20]. The black crosses in Fig. 2 are from an experiment where an artificial prepulse of contrast $10^{-5}$ is added at 40 ps prior to the main pulse. We see that no enhancement of the THz energy occurs when the target thickness is decreased from 30 to 2 $\mu$m. In fact, the peak THz energy from the 2-$\mu$m target and the $E_L = 600$ mJ laser remains below 30 $\mu$J, almost identical to that from the thicker targets and much lower than all the high-contrast-laser cases. This result clearly demonstrates the adverse effect of a preplasma on the generation of THz radiation in our scheme. Finally, we also found that a misalignment of the target by 30 $\mu$m off the laser focus results in a huge drop of the laser-to-THz radiation conversion efficiency to only ~0.1%, indirectly supporting the relationship among the density and temperature of the hot electrons and the laser intensity assumed in the model.

In summary, highly efficient generation of THz radiation from the laser interaction with a thin solid target has been demonstrated experimentally. From a high-contrast 600-mJ laser interaction with a 2-$\mu$m-thick Cu target, THz radiation with ~10.5-mJ pulse energy is obtained with a laser-to-THz radiation conversion efficiency of up to 1.7%, which is ten times higher than previous studies of the laser-solid interaction and ~1.5 times higher than the laser-driven large-size organic crystal sources [21]. It was shown that the temporal dynamics of the hot electrons can affect the sheath electron density, resulting in an increase in the accelerating sheath electric field and therefore enhancement of the THz energy with decreasing target thickness. With the recent rapid progress in target fabrication and high-contrast laser technology, the THz radiation energy can be further enhanced, for example, by using nanometer-thick targets. Since the THz radiation originates from electron deceleration and acceleration by the intense sheath field, it has good radial polarization and a symmetric distribution. Focusing of such a THz beam should result in a multi-GV/m longitudinal electric field. With the further challenge to control the field phase and waveform, such a THz source can be useful for tabletop THz-driven acceleration research [22] and other intense THz applications [23]. The measured THz power and temporal waveform may also provide an alternative diagnostic of the plasma sheath during the long-time evolution.

This work was supported by the Photon Frontier Network of the Ministry of Education, Culture, Sports, Science and Technology of Japan. H.B.Z. and M.Y.Y. would like to acknowledge the support of the National Natural Science Foundation of China (Grants No. 11475259, No. 11374262, No. 11475147, No. 11175253, and No. 91230205) and the Open Fund of the State Key Laboratory of High Field Laser Physics (SIOM). H.B.Z. and Z.M.S. would like to acknowledge support from the National Basic Research Program of China (Grants No. 2013CBA01504 and No. 2014CB339801). Z.J. would like to thank J. W. Wang and S. M. Weng for fruitful discussions and Y. Kimura for target fabrication.

[1] K. W. D. Ledingham, I. Spencer, T. McCanny, R. P. Singhal, M. I. K. Santala, E. Clark, I. Watts, F. N. Beg, M. Zepf, K. Krushelnick, M. Tatarakis, A. E. Dangor, P. A. Norreys, R. Allott, D. Neely, R. J. Clark, A. C. Machacek, J. S. Wark, A. J. Cresswell, D. C. W. Sanderson, and J. Magill, Phys. Rev. Lett. **84**, 899 (2000).

[2] E. L. Clark, K. Krushelnick, J. R. Davies, M. Zepf, M. Tatarakis, F. N. Beg, A. Machacek, P. A. Norreys, M. I. K. Santala, I. Watts, and A. E. Dangor, Phys. Rev. Lett. **84**, 670 (2000).

[3] A. J. Mackinnon, Y. Sentoku, P. K. Patel, D. W. Price, S. Hatchett, M. H. Key, C. Andersen, R. Snavely, and R. R. Freeman, Phys. Rev. Lett. **88**, 215006 (2002); S. Buffechoux *et al.*, *ibid.* **105**, 015005 (2010).

[4] H. Hamster, A. Sullivan, S. Gordon, W. White, and R. W. Falcone, Phys. Rev. Lett. **71**, 2725 (1993); H. Hamster, A. Sullivan, S. Gordon, and R. W. Falcone, Phys. Rev. E **49**, 671 (1994).

[5] G. Q. Liao *et al.*, Phys. Rev. Lett. **114**, 255001 (2015).

[6] A. Sagisaka, H. Daido, S. Nashima, S. Orimo, K. Ogura, M. Mori, A. Yogo, J. Ma, I. Daito, A.S. Pirozhkov, S.V. Bulanov, T. Z. Esirkepov, K. Shimizu, and M. Hosoda, Appl. Phys. B **90**, 373 (2008).

[7] Z. Jin, Z. L. Chen, H. B. Zhuo, A. Kon, M. Nakatsutsumi, H. B. Wang, B. H. Zhang, Y. Q. Gu, Y. C. Wu, B. Zhu, L. Wang, M. Y. Yu, Z. M. Sheng, and R. Kodama, Phys. Rev. Lett. **107**, 265003 (2011).

[8] Y. T. Li, C. Li, M. L. Zhou, W. M. Wang, F. Du, W. J. Ding, X. X. Lin, F. Liu, Z. M. Sheng, X. Y. Peng, L. M. Chen, J. L. Ma, X. Lu, Z. H. Wang, Z. Y. Wei, and J. Zhang, Appl. Phys. Lett. **100**, 254101 (2012).

[9] Z. M. Sheng, K. Mima, J. Zhang, and H. Sanuki, Phys. Rev. Lett. **94**, 095003 (2005); Z. M. Sheng, Y. Sentoku, K. Mima, J. Zhang, W. Yu, and J. Meyer-ter-Vehn, *ibid.* **85**, 5340 (2000).

[10] K. Y. Kim, B. Yellampalle, A. J. Taylor, G. Rodriguez, and J. H. Glownia, Opt. Lett. **32**, 1968 (2007).

[11] A. Gopal *et al.*, New J. Phys. **14**, 083012 (2012); A. Gopal, S. Herzer, A. Schmidt, P. Singh, A. Reinhard, W. Ziegler, D. Brömmel, A. Karmakar, P. Gibbon, U. Dillner, T. May, H. G. Meyer, and G. G. Paulus, Phys. Rev. Lett. **111**, 074802 (2013); A. Gopal, P. Singh, S. Herzer, A. Reinhard, A. Schmidt, U. Dillner, T. May, H.-G. Meyer, W. Ziegler, and G. G. Paulus, Opt. Lett. **38**, 4705 (2013).

[12] C. Bellei *et al.*, New J. Phys. **12**, 073016 (2010).

[13] The phase retardation is measured using a CCD camera with $\Delta\phi \sim \sin^{-1}(\Delta I/I) \sim 1.1\pi$. The THz field amplitude is calculated from the formula $E_{\mathrm{THz}} = \lambda\Delta\phi/2\pi\, L n_0^3 r_{41} t_{\mathrm{ZnTe}} t_{\mathrm{LPF}} t_{\mathrm{Teflon}} t_{\mathrm{TPX}}$, where $\lambda = 800\,\mathrm{nm}$ is the wavelength of probe beam, $L = 1\,\mathrm{mm}$ is the thickness of ZnTe, $n_0 = 2.87$ is the refractive index of ZnTe, $r_{41} = 4.04\,\mathrm{pm/V}$ is the electro-optical coefficient of ZnTe, $t_{\mathrm{ZnTe}} = 0.47$ is the Fresnel transmission coefficients of ZnTe, $t_{\mathrm{LPF}} = 0.36$ is the transmission of the long-pass filter, $t_{\mathrm{Teflon}} = 0.36$ is the transmission of the Teflon window, and $t_{\mathrm{TPX}} = 0.44$ is the transmission of the two TPX lenses.

[14] S. P. Hatchett *et al.*, Phys. Plasmas **7**, 2076 (2000); S. C. Wilks, A. B. Langdon, T. E. Cowan, M. Roth, M. Singh, S. Hatchett, M. H. Key, D. Pennington, A. MacKinnon, and R.A. Snavely, *ibid.* **8**, 542 (2001).

[15] H. B. Zhuo, Z. L. Chen, W. Yu, Z. M. Sheng, M. Y. Yu, Z. Jin, and R. Kodama, Phys. Rev. Lett. **105**, 065003 (2010); H. B. Zhuo, Z. L. Chen, Z. M. Sheng, M. Chen, T. Yabuuchi, M. Tampo, M. Y. Yu, X. H. Yang, C. T. Zhou, K. A. Tanaka, J. Zhang, and R. Kodama, *ibid.* **112**, 215003 (2014).

[16] J. D. Jackson, *Classical Electrodynamics*, 3rd ed. (Wiley, New York, 2002).

[17] P. Antici, J. Fuchs, M. Borghesi, L. Gremillet, T. Grismayer, Y. Sentoku, E. d'Humières, C. A. Cecchetti, A. Mančić, A. C. Pipahl, T. Toncian, O. Willi, P. Mora, and P. Audebert, Phys. Rev. Lett. **101**, 105004 (2008).

[18] M. J. Berger, J. S. Coursey, M. A. Zucker, and J. Chang, (2005), ESTAR, PSTAR, and ASTAR: Computer Programs for Calculating Stopping-Power and Range Tables for Electrons, Protons, and Helium Ions, version 1.2.3, available at http://physics.nist.gov/Star (National Institute of Standards and Technology, Gaithersburg, 2005).

[19] S. C. Wilks and W. L. Kruer, IEEE J. Quantum Electron **33**, 1954 (1997).

[20] M. Kaluza, J. Schreiber, M. I. K. Santala, G. D. Tsakiris, K. Eidmann, J. Meyer-ter-Vehn, and K. J. Witte, Phys. Rev. Lett. **93**, 045003 (2004).

[21] C. Vicario, B. Monoszlai, and C. P. Hauri, Phys. Rev. Lett. **112**, 213901 (2014).

[22] E. A. Nanni, W. R. Huang, K.-H. Hong, K. Ravi, A. Fallahi, G. Moriena, R. J. D. Miller, and F. X. Kärtner, Nat. Commun. **6**, 8486 (2015).

[23] H. Hirori, K. Shinokita, M. Shirai, S. Tani, Y. Kadoya, and K. Tanaka, Nat. Commun. **2**, 594 (2011); J. Liu, J. Dai, S. L. Chin, and X.-C. Zhang, Nat. Photon. **4**, 627 (2010); M. Liu *et al.*, Nature (London) **487**, 345 (2012).